



Full Text View

[Volume 28, Issue 12 \(December 1998\)](#)

Journal of Physical Oceanography

Article: pp. 2444–2458 | [Abstract](#) | [PDF \(215K\)](#)

Subinertial Dynamics on the Inner New Jersey Shelf during the Upwelling Season

Alexander E. Yankovsky and Richard W. Garvine

Graduate College of Marine Studies, University of Delaware, Newark, Delaware

(Manuscript received October 31, 1997, in final form February 24, 1998)

DOI: 10.1175/1520-0485(1998)028<2444:SDOTIN>2.0.CO;2

ABSTRACT

Subinertial dynamics on the inner New Jersey shelf is examined using time series of the forcing agents (atmospheric pressure, wind stress, and Hudson River streamflow), adjusted sea level (ASL) along the southern part of the Mid-Atlantic Bight, and mooring data collected during the summer of 1996.

High-frequency (period 1–3 days) transient wind-driven events were evident both in ASL and alongshelf current data. ASL events propagated southward with remarkably high speed ($\sim 10 \text{ m s}^{-1}$) in the manner of free coastally trapped waves (CTW). However, these transients were forced by the wind events within the study domain: both ASL and alongshelf current fluctuations were coherent with the local alongshore wind stress. ASL amplitude substantially increased downshelf (southward). These transient flows propagated from the corner in the coastline formed by the southern Long Island and northern New Jersey coasts. This bend of the coastline created a discontinuity in the alongshore wind stress component that caused the generation of CTW pulses at this location.

During the period of observations, enhanced buoyant flows arrived at the site of the moorings. They were associated with increased Hudson River discharge. These buoyant flows and transient wind-driven events strongly interacted: transient wind-driven currents were dramatically amplified in the buoyant water while the buoyant water was spread offshore. Amplified transient currents were not associated with the enhanced vertical shear.

Lower-frequency wind forcing generated upwelling events with typical duration of 8–10 days. During the upwelling, temperature dropped through the whole water column, but the stratification remained significant (5° – 6°C in 8–10 m of water). Even though upwelling-favorable winds dominated, record-mean currents in the upper layer were weak (2 – 5 cm s^{-1}) due to the close competition between wind and buoyancy forcing.

Table of Contents:

- [Introduction](#)
- [The dataset](#)
- [Observations](#)
- [Discussion and summary](#)
- [REFERENCES](#)
- [FIGURES](#)

Options:

- [Create Reference](#)
- [Email this Article](#)
- [Add to MyArchive](#)
- [Search AMS Glossary](#)

Search CrossRef for:

- [Articles Citing This Article](#)

Search Google Scholar for:

- [Alexander E. Yankovsky](#)
- [Richard W. Garvine](#)

1. Introduction

This study presents some results of the observational program carried out in summer of 1996 on the New Jersey shelf ([Fig. 1](#) shows the geographical location). We address two central questions in this paper. How is the subinertial dynamics on the inner New Jersey shelf related to the principal forcing agents: alongshore wind and buoyant discharge of the Hudson River? What is the role of the coastline and shelf geometry in the generation of the observed patterns of coastal dynamics?

The main purpose of the project was to consider the wind-driven dynamics on the inner New Jersey shelf during the entire summer upwelling season. A major element of the field study was an array of moored buoys deployed on the shelf between the 10-m and 25-m isobaths off Atlantic City and consisting of three across-shelf lines of moorings. In this paper we present some of the data obtained at the moorings along with time series of sea level, atmospheric pressure, wind stress, and Hudson River streamflow.

Subinertial fluctuations of the adjusted sea level (ASL) in the Mid-Atlantic Bight (MAB) and their relation to wind forcing were studied by [Noble and Butman \(1979\)](#) and [Wang \(1979\)](#). They found that the ASL fluctuations with periods greater than 3 days were coherent over the whole MAB. These ASL events were driven by the local wind in the northern part of the domain. Since the atmospheric systems propagated mainly northeastward, ASL did not exhibit clear southward phase propagation in that part of the domain [as for free coastal-trapped waves (CTW)]. In the southern part of the MAB, ASL events did propagate southward as free CTWs and had lower coherence with the local wind forcing. [Wang \(1979\)](#) also showed that the ASL events with periods shorter than 3.3 days were coherent (and forced by the local wind) along the southern part of the MAB and were not coupled to the fluctuations in the northern part.

[Ou et al. \(1981\)](#) and [Noble et al. \(1983\)](#) examined the subinertial variability of the currents in the MAB. Ou et al. considered subinertial dynamics in the MAB in terms of forced wave propagation upshelf (northward) along with the atmospheric systems and free wave propagation downshelf (southward). Noble et al. also partitioned alongshelf currents into wind-forced motions and freely propagating waves, which together explained 75%–90% of the observed subinertial current energy. They found that the contribution of the forced component became relatively more important at the southern edge of their observational array. Since both papers were based on observations carried out on the mid-to-outer shelf (60-m depth and deeper), no evidence of a buoyancy-driven component was presented.

[Doyle and Wilson \(1978\)](#) examined the structure of the Hudson River buoyant inflow into the New York Bight across a section from Sandy Hook to Rockaway Point. Observations of the Hudson River plume spreading in the New York Bight Apex were presented by [Bowman \(1978\)](#). Under upwelling-favorable (upshelf) wind, discharge spread radially offshore as a thin lens, forming an anticyclonic plume attached to the mouth, while under downwelling-favorable wind the buoyant current was narrower and propagated downshelf along the coast. [Münchow \(1992\)](#) demonstrated that the Hudson River buoyant plume under conditions of high runoff can propagate along the New Jersey shelf south of Atlantic City.

In the following study we will consider some principal elements of the subinertial dynamics on the inner New Jersey shelf including transient wind-driven currents, upwelling events, and the arrival of buoyant plumes and their interactions. We will start with data description, then examine the forcing agents and the large-scale barotropic response of the coastal flow (which exhibits itself in sea level), and then proceed with the analysis of time series obtained at the moored buoys.

2. The dataset

In this paper, we study subinertial dynamics in the southern part of the Middle Atlantic Bight from Long Island southward. For this purpose, we obtained wind, atmospheric pressure, and sea level data at stations representing this region, as well as Hudson River streamflow data.

a. Atmospheric forcing

Wind and atmospheric pressure data were measured at hourly intervals at JFK airport, New York (station NY), Atlantic City, New Jersey (AC), and Norfolk, Virginia (NF). We estimated the vector wind stress $\boldsymbol{\tau}$ as

$$\boldsymbol{\tau} = \rho_a C_a |\mathbf{W}| \mathbf{W}, (1)$$

where ρ_a is the air density, C_a is the wind stress coefficient, and \mathbf{W} is the wind velocity. In general, C_a increases with the wind speed ([Wu 1980](#)). However, typical magnitude of the wind speed during the period of observations was only 5–8 m

s^{-1} . With $\rho_a = 1.2 \text{ kg m}^{-3}$ and $C_a = 1.25 \times 10^{-3}$ for this range of wind speed, we approximate the wind stress (Pa) as $1.5 \times 10^{-3} |\mathbf{W}|W$ (where \mathbf{W} is measured in m s^{-1}). [Sandstrom \(1980\)](#) used the same expression for wind stress estimation.

We consider the alongshore component of the wind stress as the principal forcing. However, the coastline bends substantially near stations NY and NF. Thus, we derived *two* alongshore wind stress time series for both NY and NF. For NY we chose the direction 8° ccw from east to represent the alongshore direction for the southern coast of Long Island, while we chose 81° for the northern New Jersey coast. For NF we chose 60° for the coast north of Cape Henry and 103° for the coast to the south. For AC we selected 51° . Data from 1 May through 31 August were analyzed, as this time interval overlaps the duration of the field observations and represents the summer upwelling season.

b. Buoyant discharge

Since direct measurements of the Hudson River freshwater discharge into the New York Bight Apex are not available, we used the Hudson River streamflow data at Waterford, New York. This is the southernmost available station not affected by tides. There is substantial delay between the signal at Waterford and the arrival of enhanced buoyancy off Atlantic City; [Münchow \(1992\)](#) found that it exceeded one month. Thus, we analyzed streamflow data from 1 April through 31 August.

c. Sea level

We obtained hourly tide gauge data at six stations from Montauk, New York, down to Duck, North Carolina ([Fig. 1](#) shows the station locations). Among available stations, we chose those that are located on straight, regular coastlines, when possible. Sea-level time series presented here span the period from 1 May through 31 August.

d. Time series from moorings

For the purpose of this study, we analyzed data from only three moorings (N1, S1, and S3; see [Fig. 1](#)) where Inter Ocean S4 current meters were deployed. These provided time series of water velocity, temperature, and conductivity. Data were obtained at depths 2, 4, and 8 m (N1); 2 and 10 m (S1); 9, 16, and 23 m (S3) for the period 19 May through 15 August with a 5-min average for every 30-min sampling interval. We used the principal axis component as representative of the alongshelf direction for current because the coastline is not parallel to the local isobaths within the study site. We define the downshelf direction as that of Kelvin wave propagation, with upshelf as the opposite direction.

e. Data analysis

All time series were low-pass filtered with a Lanczos filter (35-h cutoff period). Sea level data were adjusted to atmospheric pressure. Since the low-frequency subinertial atmospheric pressure was similar at all three locations, we used NY pressure data to adjust sea level at Montauk and Sandy Hook, AC pressure at Atlantic City and Lewes, and NF pressure at Wachapreague and Duck. We observed energetic motions with periods close to inertial; thus, raw data for wind stress and currents were used for spectral analysis. All time series were sampled at 1-h interval. We cut the time series of sea level and wind into overlapping sections of length 512 h resulting in 16 effective degrees of freedom, while we cut the time series of currents into sections of length 256 h (since these time series were shorter) with 23 effective degrees of freedom.

3. Observations

a. Forcing

Time series of the low-pass filtered atmospheric pressure at NY, AC, and NF show that the data from these different locations are in general similar; thus, the same atmospheric processes dominated the whole study domain. However, high-frequency events with durations of 1 to 2 days (high-frequency limit of the “weather” band) exhibit some differences at the different locations. Time-lagged cross-correlation coefficients for the pairs of time series (AC and NY; AC and NF) reveal that, on average, atmospheric systems moved upshelf along the coast (in the northeast direction). Maximum value of the cross-correlation coefficient for AC and NF was 0.96; for AC and NY it was 0.74.

Low-pass filtered time series of the alongshore wind stress are presented in [Fig. 2](#) as measured at NY, both for the Long Island (NY/LI) and New Jersey (NY/NJ) coasts, at AC, and at NF (only to the north of Cape Henry, NF/N). In general, weak to moderate winds prevailed with few events when the alongshore component exceeded 0.1 Pa. The weakest alongshore wind stress was observed at AC ([Fig. 2b](#)), the nearest station to the mooring sites. Upwelling-favorable (upshelf) wind stress dominated during the period of observations (positive values in [Fig. 2](#)). Compared to atmospheric pressure, alongshore wind stress had greater high-frequency variability (wind events with period of 1–3 days) and also clearer differences between time series at different locations. Over the whole period of the observations, wind events did not

show a clear tendency for alongshore propagation. Cross-correlation coefficients between upwelling time series were 0.6–0.8 with the time lag for maximum correlation of ± 1 –2 h (depending on the particular pair). Correlation between NY/LI alongshore wind stress and all other wind stress time series was low (maximum absolute values were less than 0.2). For time series NY/NJ and NF/S, the northern and southern extremes of the domain, maximum cross-correlation coefficient was 0.61 with 0-h time lag. Power spectra of the alongshore wind stress (NY and AC; [Fig. 3](#)) show a strong diurnal signal, especially for the New Jersey coast. Another spectral peak appears at frequencies 0.3–0.4 cycles per day (cpd). NY/NJ wind stress had the highest spectral density for high-frequency oscillations, while NY/LI wind stress had the highest spectral density at low frequencies (< 0.3 cpd). Among the three time series, AC had the lowest spectral density at all frequencies.

We chose the running integral of the AC alongshore wind stress component over time ([Fig. 4](#)) as a measure in time of upwelling favorable conditions, $T_i(t)$. We use the AC time series because this wind stress is the local one for the site of observations. The integration begins on yearday (yd) 92 (1 April). We infer that active upwelling occurred during those periods of time when T_i increased monotonically. For other times the upper-layer flow should have been turned downshelf by the buoyancy forcing. We infer from [Fig. 4](#) that the upwelling season continued from mid-April through early August and contained at least five periods of upwelling favorable wind events lasting 8–12 days.

Hudson River streamflow at Waterford ([Fig. 5](#)) was high from yd 105 (mid-April) through yd 145 (late May) with two absolute maxima on yd 108 and 134. Taking into account the approximate 40 day's delay for the discharged buoyancy to arrive at AC, we estimate that enhanced buoyant flow was present on the inner New Jersey shelf at least through yd 185 (beginning of July).

b. Sea level

Time series of the low-pass filtered, adjusted sea level from Montauk down to Duck show the existence of pronounced, high-frequency fluctuations with periods 1–3 days ([Fig. 6](#)). Their amplitude was fairly small at Montauk, but substantially increased downshelf between Sandy Hook and Duck. As examples, three distinguishable pulses are marked with vertical dotted lines. Evidently, these were transient events that propagated downshelf. We estimated space- and time-lagged cross-correlation coefficients ([Allen and Denbo 1984](#)) between ASL at AC and the other stations ([Fig. 7](#)). These coefficients indicate that the ASL fluctuations were well-correlated within the study domain. [Figure 7](#) also shows a tilt in the contours (especially downshelf from AC), that is, fluctuations at AC led fluctuations southward. We added a line representing the locus of maximum correlation. Its slope indicates the propagation speed of ASL fluctuations along the coast. Taking the alongshore distance between the AC and DK stations as 405 km and the corresponding time lag as 12 h, the propagating speed for ASL was $\sim 10 \text{ m s}^{-1}$. This value is in agreement with the crude estimation for a nondispersive barotropic shelf wave (BSW) phase speed, $C = fL$, where f is the Coriolis parameter and L is the shelf width. For the southern part of the MAB, $L \sim 120 \text{ km}$ and $f \sim 0.9 \times 10^{-4} \text{ s}^{-1}$, giving $C = 10.8 \text{ m s}^{-1}$. The ASL propagation speed tended to decrease at the downshelf edge of the domain, which might be explained by the narrowing shelf.

Power spectra of ASL at Montauk, Atlantic City, and Duck are presented in [Fig. 8a](#). At the high-frequency limit (frequencies greater than 0.7 cpd), the energy of the fluctuations goes down abruptly because here we used low-pass filtered time series for spectral analysis. In general, energy increases downshelf, as is also obvious from a visual analysis of the ASL time series ([Fig. 6](#)). From MT to AC, energy increases at nearly all frequencies. From AC to DK, energy remains the same at the low frequencies (0.1 cpd and lower) but gains the highest increase at frequencies 0.3–0.4 cpd. Within this latter frequency band, the energy of ASL fluctuations at DK exceeds that at MT by more than one order of magnitude.

Since the ASL fluctuations propagated downshelf while gaining additional energy, we estimated the coherence squared of ASL at a southern location (WP) with all other stations. We used WP rather than DK (southernmost) station because the shelf is relatively straight and uniform from NY to WP. From WP to DK, the coastline bends and the shelf narrows, which may cause some distortion (scattering) of the propagating wave. Lower-frequency fluctuations (< 0.3 cpd) were coherent through the entire domain, consistent with previous studies ([Wang 1979](#); [Noble and Butman 1979](#)). We are particularly interested, however, in the high-frequency subinertial transient events (periods 1.5–3 days). [Figure 8b](#) demonstrates that the ASL fluctuations at WP within this frequency range were coherent with the upshelf ASL up to Atlantic City–Sandy Hook. It is especially true for the most energetic motions at frequency 0.35–0.4 cpd: coherence was high from DK up to AC (> 0.6) but went down abruptly at SH and remained at a substantially lower level (0.3–0.4) at MT. Qualitatively similar plots were obtained when we used AC, LW, or DK (rather than WP) stations. The main conclusion is that the high-frequency ASL events maintained high coherence between different stations while traveling southward from SH. Based on this fact, we suggest that these features propagated from the New York Bight Apex, that is, from the “corner” formed by the northern New Jersey and southern Long Island coasts.

[Figure 9](#) shows how the observed ASL fluctuations were related to the alongshore wind stress within the study domain. For this purpose, we estimated coherence squared between ASL at DK (downshelfmost location) and all available

alongshore wind-stress time series. Sea level at DK was highly coherent with the wind stress at NF at all frequencies. Interestingly, at low frequencies coherence was higher with alongshore wind stress relative to the coast north of Cape Henry (NF/N) rather than to the coast south (NF/S), even though the latter was more “local” for DK. Perhaps this occurred because the low-frequency oscillations were driven by wind forcing on the domain scale for which the effective orientation of the coastline happens to coincide with that north of Cape Henry.

High-frequency ASL fluctuations (0.3–0.7 cpd) had significant coherence with the upshelf wind stress at AC and NY/NJ, especially at frequencies 0.3–0.4 cpd. The sharp bend in the coastline at the New York Bight Apex abruptly changed the *alongshore* component of the wind stress (even though the wind stress itself remained the same). As a result, ASL fluctuations were not coherent with the alongshore wind stress NY/LI (except for frequencies 0.4 and 0.6 cpd, which we will discuss next). Thus, there is an effective “cutoff” of the wind forcing for high-frequency ASL events propagating along the southern part of the MAB. This cutoff occurs at the New York Bight Apex where the coastline abruptly changes its orientation.

In several cases, short-period wind events (typical duration 1–2 days) exhibited themselves simultaneously both in the NY/LI and NY/NJ alongshore wind components with the same sign, that is, both were either upwelling-favorable or downwelling-favorable (Fig. 2). Then enhanced disturbances of the sea surface occurred at the corner of the New York Bight Apex (compared to both up- and downshelf locations) where the joint effect of two alongshore wind components was combined. This, in turn, caused the generation of higher amplitude pulses that propagated from this corner downshelf. Indeed, Fig. 10 shows two examples of ASL transient events that propagated from Sandy Hook to Duck and clearly were triggered by the joint effect of NY/NJ and NY/LI alongshore wind stress events. These two ASL pulses had higher amplitude than other ASL events driven by an even stronger alongshore wind stress component, but acting singly (NY/NJ). Thus, the appearance of ASL fluctuations at DK having significant coherence with NY/LI alongshore wind fluctuations at frequency 0.4 and 0.6 cpd might be associated with this mechanism.

Based on Fig. 10 (dashed lines AB), we inferred the propagating speeds through the domain for these two events. For the first case (Fig. 10, left panel), the average speed was 7.5 m s^{-1} , while for the second case (Fig. 10, right panel) it was 11 m s^{-1} . This speed difference might be due to different modal structures for the two pulses.

In summary, high-frequency (period 1.5–3 days) ASL events propagated downshelf (southward) with a speed typical of freely propagating BSWs. At the same time, ASL fluctuations were coherent with the alongshore winds within the study domain, suggesting local forcing. As mentioned above, neither atmospheric pressure nor alongshore wind exhibited clear southward propagation. These ASL transient events originated from the New York Bight Apex and gained amplitude while traveling from Sandy Hook to Duck. Thus, they combined features of free BSWs and forced response. We will discuss a possible mechanism for the generation of these transients in section 4.

c. Currents

Current measurements at moorings N1 (2- and 4-m depth), S1 (2-m depth), and S3 (9-m depth) were analyzed to infer some basic properties of the shelf flow subinertial response to the wind and buoyancy forcing discussed above.

Even though upwelling favorable winds prevailed during the period of measurements, record-mean currents in the upper layer were small at all locations with speeds 2–5 cm s^{-1} . This was evidently due to the close competition between buoyancy forcing (driving flow downshelf) and prevailing upshelf winds. In fact, the mean flow at N1 (both at 2 and 4 m) was directed downshelf while the mean flow at S1 (2 m) and S3 (9 m) was upshelf, probably because the across-shelf density gradient was weaker at the southern moorings compared to the northern ones (farther from the source of buoyancy). This mean flow convergence in the upper layer could produce additional offshore advection of buoyant water.

Principal axis components had the following orientations: 34° from true north at N1, 2 m; 27° at N1, 4 m; 63° at S1, 2 m and 67° at S3, 9 m (Fig. 1b). The minor difference in angles between 2 and 4 m at N1 mooring is consistent with stronger offshore Ekman drift in the upper layer caused by the prevailing upshelf winds. The principal axis angles were nearly parallel to the local coastline and isobaths (Fig. 1). Most of the variability along the minor axes was associated with tidal currents. Harmonic analysis showed that, in general, tides were weak and their amplitude decreased northward. Diurnal tidal constituents had an amplitude 2–4 cm s^{-1} at both northern and southern locations while the amplitude of the semidiurnal M_2 constituent increased from 1 cm s^{-1} at N1 to 9 cm s^{-1} at S1 and 13 cm s^{-1} at S3.

Figure 11 shows the low-pass filtered time series of “alongshelf” (principal axis) currents at S1, 2 m and S3, 9 m along with the water density measured at the same locations plus S3, 23 m. Since the wind stress is an important forcing agent, two time series (NY/NJ and AC) are shown again for reference.

transient wind-driven events (periods 1.5–3 days) that exhibited differences in ASL were also apparent in alongshelf current time series and corresponded to particular wind events. However, their amplitude on the inner shelf (S1, 2 m; solid curve in Fig. 11b) changed remarkably through the period of observations. They had strongest amplitudes from yd 149 through 160 (early June) and again from yd 168 to 185 (the second half of June through the beginning of July). The wind events tended to be of the same magnitude throughout the season. But the transient currents on the inner shelf (solid curve in Fig. 11b) became much stronger during the two periods when lower water density was present on the inner shelf. Then the corresponding density difference between shoreward (S1) and seaward (S3) moorings was greater. We use vertical dashed lines and cross-hatching to mark these time intervals in Fig. 11. Thus, the two appearances of enhanced buoyancy corresponded to dramatically amplified transient wind-driven currents for the inner-shelf water. This was especially true for the second arrival of buoyant flow (yd 170–186) when the lowest density and the greatest density difference were observed throughout the whole study period. Wind forcing was not particularly strong then. For instance, the alongshelf wind stress was stronger during yd 190–203, but the response of the shelf flow was much weaker (due to lack of an across-shelf density difference). Farther offshore (mooring S3), the transient wind-driven current was weak and did not exhibit such amplitude modulation when the buoyant water was present onshore.

We infer that these two enhanced events were caused by the higher discharge of the Hudson River in mid-April through late May (Fig. 5). The second event was particularly strong for the following reason. Before the second arrival of buoyant flow, moderate upwelling favorable winds persisted for more than 10 days (yd 156 through 167—Fig. 11a), blocking downshelf spreading of buoyant flow and allowing the accumulation of fresh water in the New York Bight Apex. Thus, when the upshelf wind ceased blowing, this buoyant water with a strong across-shelf density gradient started to move downshelf.

The structure of the buoyant flow was in turn modified by the transient currents. Observations from yd 170 through 182 (during the second and most intense period of buoyancy difference) show that the density at the coast reached its minimum on yd 173 (Fig. 11c), then began to increase while the density offshore (S3 at 9 m) continued to decrease. The same tendency was observed for the vertical structure of the buoyant layer at the inner shelf moorings (only S1 is shown as an example in Fig. 12): after the core of the buoyant water arrived, the surface density gradually increased while bottom density kept decreasing. Indeed, surface and bottom density almost merged by yd 180. To demonstrate the importance of the transient wind-driven currents, we show raw data in Fig. 12. While the surface density fluctuations had some higher-frequency noise (solid curve in Fig. 12), both density records have dominating scales of 1–2 days. Thus, we deduce that the transient wind-driven flows were the major agent for the short-term density variability. Meanwhile, vertical stratification at S3 between 9 and 23 m became even greater (compare dashed and dotted lines in Fig. 11c) due to offshore spreading of buoyancy in the upper layer. Thus, buoyancy was spread offshore and the across-shelf density difference in the upper layer decreased (solid and dashed lines converge in Fig. 11c), when transient currents propagated through the buoyant water. This conclusion is further supported by the absence of persistent upwelling-favorable wind stress during this period. The latter is often assumed to be a principal agent for offshore spreading of buoyancy.

We emphasize that the observed enhanced currents in the buoyant layer were caused by the interaction of the buoyancy and wind-driven currents (rather than solely due to any “patchy” spatial structure of the plume or its instability). Indeed, Fig. 13 (upper panel) shows that the buoyant flow propagated relatively slowly along the coast, taking several days to move from mooring N1 south to S1 (38 km apart). Thus, any small-scale features of the buoyant flow would exhibit themselves at S1 a few days later than at N1. In contrast, the current oscillations were nearly in phase at N1 and S1 and corresponded to ASL oscillations at Atlantic City. ASL represents the barotropic response of the shelf flow and has a large alongshelf scale (Fig. 6), so it should be almost identical at N1 and S1. Thus, the wind-driven transient barotropic response sets up the timing or phase, while the buoyant layer enhances the amplitude of the transient currents on the inner shelf. Furthermore, the amplitude of alongshelf velocity fluctuations was almost identical at both locations after yd 174 (Fig. 13), that is, after the buoyant flow arrived both at N1 and S1. Since details of the density disturbances differed substantially at N1 and S1, we assume that the observed amplification of alongshelf currents was a more complicated process than just a local response of the buoyant layer to the wind stress.

In Fig. 13 we compare alongshelf currents at N1 and S1 with ASL rather than with the wind stress because the coastline and isobaths have different orientation at N1 and S1. As a result, local alongshore wind stress should be different at N1 and S1. In fact, the spacial orientation of the principal axes at N1 and S1 for 2-m depth differs by almost 30°. ASL response is spatially smoother alongshore than the alongshore wind stress. Recall that the correlation for ASL between different stations was higher than for alongshore wind stress.

Next we consider how the presence of buoyancy influenced the vertical structure of the transient currents. Figure 14b shows a low-pass filtered difference ($V_2 - V_4$) between principal axis velocities at 2 and 4 m, mooring N1, during yd 143–180. We normalized this difference by the absolute value of the vertically averaged alongshelf velocity in this layer: $(0.5|V_2 + V_4|)^{-1}$, where V is an alongshelf (principal axis) velocity component and the subscript denotes the instrument depth. For reference, we plot V_2 in Fig. 14 to show the time intervals when enhanced transient currents occurred.

In general, there was no tendency for vertical shear to increase with increased buoyancy. Time series of water density (Fig. 14c) show two arrivals of buoyant water. When buoyant flow arrived the second time (after yd 167—Fig. 14c), its vertical structure gradually changed over time. At first buoyant flow was trapped at the surface, then the buoyant layer gradually deepened and, finally, occupied the whole water column by yd 178. However, the vertical density difference did not cause any increase in the vertical shear of the alongshelf velocity. On the contrary, enhanced transient currents had more uniform vertical structure than otherwise. From yd 168 through yd 172, the density difference between depth 2 and 4 m was in the range $1\text{--}3\text{ kg m}^{-3}$, yet the nondimensional “shear” in this layer (Fig. 14b) was close to zero. The normalized vertical difference of the alongshelf velocity was stronger during the upwelling event (yd 155–166, Figs. 14b,c) when buoyant flow was not present on the inner shelf.

These results have the following implications: amplification of transient currents was not simply caused by the concentration of wind-induced momentum in the shallow buoyant layer or by the enhanced vertical (geostrophic) shear associated with the greater cross-shelf density difference. The alongshore current response was not surface intensified, it was present throughout the water column.

Throughout the period of the mooring observations, three major upwelling events occurred (Fig. 15a). There were no persistent downwelling favorable wind events. Typical duration of upwelling events was 8–10 days. These events corresponded to the period of time when the upwelling measure T_i grew steadily, that is, offshore Ekman transport was constantly maintained.

The response of the temperature field during these upwelling events was clear. We use temperature rather than density as an indicator for the upwelling events because it was more sensitive to across-shelf transport. There was approximately one day delay in the temperature response of the upper layer compared to the lower. During the upwelling events, temperature on the inner shelf dropped through the whole water column, but the temperature difference between bottom and surface layers remained substantial and even tended to grow. For instance, by the end of the first upwelling event (yd 165–166) the temperature difference between the 2-m and 8-m depth at N1 mooring was $5^{\circ}\text{--}6^{\circ}\text{C}$ (Fig. 15b).

Spectral analysis of the alongshelf current time series demonstrates the difference between the high-frequency (period 1–3 days) and low-frequency (period 7–10 days) response. The power spectrum (Fig. 16a) of the alongshelf velocity at N1, 4-m depth shows relatively uniform energy level for subinertial fluctuations. However, the vertical shear of the alongshelf velocity between 2 and 4 m was more frequency dependent and grew toward the lower frequencies. Alongshelf velocity fluctuations were coherent with the upshelf (NY) winds only within the high-frequency band (0.6–1 cpd); coherence with AC (local) alongshore wind was also high only for high frequencies, but for a wider frequency band (0.3–1 cpd) (Fig. 16b). Alongshelf currents were coherent with the winds at diurnal frequency. Wind power spectra had strong peaks at this frequency. We infer that these diurnal fluctuations of alongshelf currents were not of tidal origin solely, but contained a substantial wind-driven component, perhaps associated with a sea-breeze circulation. Spectral density of the temperature fluctuations at the same point grew toward the low frequencies and the coherence between temperature and local (AC) wind was high both at high frequencies (0.65–1 cpd) and at low frequencies (<0.3 cpd) (Fig. 17).

In these estimations, we used alongshore wind itself as a representative of the wind forcing. Even though the wind stress is dynamically important and appears in the momentum balance equation, we found the wind to be more coherent with the response (especially for alongshelf current). The same outcome was reported in several previous studies: Sandstrom (1980), Garrett and Toulany (1981, 1982).

Thus, high-frequency fluctuations of currents were coherent with the alongshore wind and were more vertically uniform while the low-frequency currents had stronger vertical shear and had lower coherence with the winds. We conclude that lower-frequency variability of currents was more baroclinic and was related to the changes in the density field. These fluctuations of density had a more complicated nature because (i) wind-forcing caused both mixing and advection and (ii), while temperature fluctuations were coherent with the local wind, salinity also depended on the fluctuations of the Hudson River runoff.

4. Discussion and summary

Wind forcing over the southern part of the Mid-Atlantic Bight (from the New York Bight Apex to Duck) during the summer season of 1996 was upwelling-favorable and produced substantial subinertial variability of the currents on the inner New Jersey shelf. High-frequency wind fluctuations (1.5–3 days) generated transient events evident both in ASL and in alongshelf velocity of inner shelf currents. Clarke and Brink (1985) showed that the response of such a wide, midlatitude shelf to fluctuating wind forcing should be barotropic. Schwing (1992) demonstrated that this was true for the subtidal Scotian Shelf circulation: inside the 100-m isobath wind driven currents with periods 2–5 days were predominantly barotropic. Beardsley et al. (1985) showed that the subinertial currents were depth independent on the shelf south of Nantucket. In our case, wind-driven (presumably barotropic) transient currents interacted with a buoyant flow on the inner

shelf. During two periods of time enhanced flows arrived at the site of the observations that caused dramatic amplification of the transient currents in the buoyant water. However, this amplification was not associated with the trapping of the wind-induced momentum in the shallow buoyant layer or with greater vertical shear of the transient currents due to across-shelf density gradient. Instead, we found that the normalized vertical shear of the alongshelf velocity actually decreased during the most dramatic amplification of the transient currents. Thus, we argue that the interaction of wind-driven barotropic transients with buoyant coastal flow leads to this remarkable amplification of currents.

We propose an explanation for this phenomena based in part on the results of [Yankovsky and Chapman \(1996, 1997\)](#). When subinertial barotropic transients propagate along the shelf in the presence of a spatially nonuniform mean current, the linearized vorticity equation takes the form ([Yankovsky and Chapman 1996](#))

$$\xi_t + \text{Ro}[(U\xi)_x + (V\xi)_y] + J(\psi, P) = 0, (2)$$



where ξ and ψ are the relative vorticity and streamfunction (associated with the transient flows), $P = [1 + \text{Ro}(V_x - U_y)]/h$ is the background (undisturbed state) potential vorticity, U and V are the horizontal components of a mean (steady state) current, h is the depth, and Ro is the nondimensional Rossby number. Subscripts denote partial differentiation and J indicates the Jacobian operator. For simplicity, we consider only free motions (no forcing term appears in the right side of the equation). Since the buoyant flow persists over a longer time than the typical duration of the observed transients, we can consider the buoyant current as the “mean” (lower frequency) current. Barotropic transient events over the southern part of MAB have much greater spatial scale than the typical buoyant plume. Thus, changes in the horizontal shear of the buoyant flow introduce substantial alongshelf disturbance in the background potential vorticity distribution on the shelf for the propagating barotropic transients. The adjustment of these transients to the alongshelf potential vorticity disturbance (associated either with the mean current or topography) should occur through the generation of intensive mesoscale flows with spatial scale comparable with this disturbance ([Yankovsky and Chapman 1997](#)). When propagating transients are considered in terms of the BSW modes, high-amplitude evanescent modes provide this adjustment ([Yankovsky and Chapman 1996](#)). These evanescent modes are trapped within the irregularities of the coastal waveguide and decay both up- and downshelf.

Other explanations are possible too. Relative vorticity could be generated within the buoyant flow due to the vertical component of the baroclinicity vector [see chapter 8 in [Gill \(1982\)](#) for details]. However, we did not observe similar amplification caused by the interaction of barotropic tides with buoyant flow.

As emphasized in the previous section, transient wind-driven events observed along the southern part of the MAB combined the properties of free waves and forced response. They propagated in the manner of free waves, unlike the forcing, yet were driven by the local winds. We suggest that the sharp bend in the coastline at the New York Bight Apex (the corner between the southern Long Island coast and the northern New Jersey coast) is responsible for that. This corner creates a discontinuity in the *alongshelf* wind stress even if the wind field is spatially uniform. The discontinuity in the wind forcing generates a wave pulse traveling downshelf from this corner.

[Carton \(1984\)](#) considered the response of the coastal ocean to the impact of an isolated storm when the wind forcing had abrupt alongshelf boundaries. In his example 3 with the wind shaped like a “top hat” both in time and alongshore direction, Kelvin waves were generated at both up- and downshelf boundaries of the forcing region at the initial moment when the wind was turned on. Within the forcing region, the disturbance grew linearly in time until the wave from the upshelf edge arrived. After that the disturbance remained constant until the end of the storm event. Thus, the location where the response reached its constant value travelled downshelf with the free wave speed. The maximum strength of the response increased downshelf within the forcing region due to delay of the wave arrival from the upshelf edge. Carton also provided more realistic numerical examples, including continuous stratification and bottom topography, along with a smooth shape for wind forcing. These agents caused more complicated multimodal responses, but the basic features of the response remained the same: generation of waves at the edges of the forcing region and propagation of the signal downshelf with increasing amplitude within the forcing region.

This physics could be relevant to our observational examples. When a particular wind event begins, discontinuity in the alongshelf wind at the corner triggers a wave pulse that propagates downshelf with free wave speed. When this wave arrives at some location, it sets up an alongshelf pressure gradient there, affecting the response to local wind forcing. Because of the wide shelf (exceeding 100 km), the propagation speed is high and the pulse travels through the domain in less than one day, less than the typical wind event duration.

[Figure 18](#)  presents evidence for this interpretation. We suggest that during every particular wind event an arrival of alongshelf pressure gradient with the wave pulse from SH sets the timing for the local response. As an example, we consider WP. We approximate the alongshelf pressure gradient which controls the response at WP as the difference in ASL fluctuations between WP and SH. For demonstrational purposes we also approximate the “local” alongshelf pressure gradient as the ASL fluctuation difference between DK and LW (i.e., a central difference). [Figure 18a](#)  shows that the

cross-correlation coefficient between ASL at WP and “alongshelf gradient” fluctuations is substantially higher when the latter is approximated as the ASL difference between WP and SH. But what is more important, the time lag of maximum correlation for this estimation is almost zero. This means that the maximum disturbance of ASL at WP occurs exactly at the time when the sea level slope between WP and SH is also greatest. Furthermore, ASL fluctuations at WP correlate even better with ASL difference between WP and SH than with the local alongshore wind stress (NF/N)—see Fig. 18b. Absolute value of the maximum cross-correlation coefficient for the former pair of time series is 0.73, while for the latter it is 0.64. The negative values on Fig. 18b mean that the upshelf wind stress causes a drop in ASL.

Thus, observed high-frequency transients along the southern part of the MAB represent the response to the wind forcing in this subdomain. But the timing and strength of the response is controlled not only by the local wind stress but also by the alongshelf pressure gradient that is carried downshelf from the New York Bight Apex by the wave pulse. This explains the observed propagating properties of these transients and the growth of their amplitude southward.

Low-frequency forcing caused a more baroclinic response in the form of upwelling events. We integrated alongshore wind in time and showed that upwelling events developed when this integral monotonically grew over a several day period, that is, under the influence of persistent upwelling favorable winds. Typical duration of upwelling events was 8–10 days. During the upwelling events, temperature dropped through the whole water column, but the vertical stratification remained substantial. This contrasts with observations on the northern California inner shelf (Lentz 1994) where vertically uniform temperature was observed during the upwelling season. Strong buoyancy forcing associated with the Hudson River discharge opposed the upwelling wind and generated downshelf flow on the inner shelf when the upwelling wind ceased.

Enhanced buoyant layers were subjected to offshore spreading. Since there were no persistent upwelling-favorable winds during the second arrival of enhanced buoyancy and tidal currents were weak, we conclude that the transient wind-driven currents were at least partly responsible for this offshore spreading of the buoyant water.

Record mean currents in the upper layer were weak ($2\text{--}5\text{ cm s}^{-1}$). We conclude that this was due to the nearly balanced competition between prevailing upshelf winds and buoyancy forcing (driving downshelf flow). The two elements of this competition were stronger during the first half of the period of observations, when both buoyancy discharge was greater and the upshelf wind was more persistent.

Acknowledgments

We are indebted to David Chapman, Steven Lentz, and Andreas Münchow for their stimulating comments and suggestions. Our work was supported by the U.S. National Science Foundation through Grant OCE-9521102. The field observational program off the New Jersey coast was a joint effort with Andreas Münchow and Scott Glenn of Rutgers University. We appreciate the cheerful and competent work of the captain and crew of the R/V *Cape Henlopen* and of Timothy Pfeiffer. Finally, special thanks to Todd Sanders for technical assistance with data processing.

REFERENCES

- Allen, J. S., and D. W. Denbo, 1984: Statistical characteristics of the large-scale response of coastal sea level to atmospheric forcing. *J. Phys. Oceanogr.*, **14**, 1079–1094.
- Beardsley, R. C., D. C. Chapman, K. H. Brink, S. R. Ramp, and R. Schlitz, 1985: The Nantucket Shoals Flux Experiment (NSFE79). Part 1: A basic description of the current and temperature variability. *J. Phys. Oceanogr.*, **15**, 713–748.
- Bowman, M. J., 1978: Spreading and mixing of the Hudson River effluent into the New York Bight. *Hydrodyn. Est. Fjords*, **23**, 373–386.
- Carton, J. A., 1984: Coastal circulation caused by an isolated storm. *J. Phys. Oceanogr.*, **14**, 114–124.
- Clarke, A. J., and K. H. Brink, 1985: The response of stratified, frictional flow of shelf and slope waters to fluctuating, large-scale, low-frequency wind forcing. *J. Phys. Oceanogr.*, **15**, 439–453.
- Doyle, B. E., and R. E. Wilson, 1978: Lateral dynamic balance in the Sandy Hook to Rockaway Point transect. *Estuar. Coast. Shelf Sci.*, **6**, 165–174.
- Garrett, C., and B. Toulany, 1981: Variability of the flow through the strait of Belle Isle. *J. Mar. Res.*, **39**, 163–189.
- and —, 1982: Sea level variability due to meteorological forcing in the Northeast Gulf of St. Lawrence. *J. Geophys. Res.*, **87**, 1968–1978.

Gill, A. E., 1982: *Atmosphere–Ocean Dynamics*. Academic Press, 662 pp..

Lentz, S. J., 1994: Current dynamics over the Northern California inner shelf. *J. Phys. Oceanogr.*, **24**, 2461–2478..

Münchow, A., 1992: The formation of a buoyancy driven coastal current. Ph.D. dissertation, University of Delaware, 205 pp..

Noble, M., and B. Butman, 1979: Low-frequency wind-induced sea level oscillations along the east coast of North America. *J. Geophys. Res.*, **84**, 3227–3236..

—, —, and E. Williams, 1983: On the longshelf structure and dynamics of subtidal currents on the eastern United States continental shelf. *J. Phys. Oceanogr.*, **13**, 2125–2147..

Ou, H. W., R. Beardsley, D. Mayer, W. C. Boicourt, and B. Butman, 1981: An analysis of subtidal current fluctuations in the Middle Atlantic Bight. *J. Phys. Oceanogr.*, **11**, 1383–1392..

Sandstrom, H., 1980: On the wind-induced sea level changes on the Scotian Shelf. *J. Geophys. Res.*, **85**, 461–468..

Schwing, F. B., 1992: Subtidal response of Scotian Shelf circulation to local and remote forcing. Part I: Observations. *J. Phys. Oceanogr.*, **22**, 523–541..

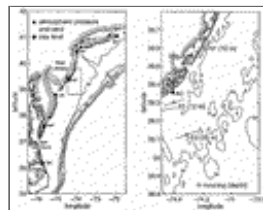
Wang, D.-P., 1979: Low frequency sea level variability on the Middle Atlantic Bight. *J. Mar. Res.*, **37**, 683–697..

Wu, Ji., 1980: Wind-stress coefficients over sea surface near neutral conditions—A revisit. *J. Phys. Oceanogr.*, **10**, 727–740..

Yankovsky, A. E., and D. C. Chapman, 1996: Scattering of shelf waves by a spatially varying mean current. *J. Geophys. Res.*, **101**, 3479–3487..

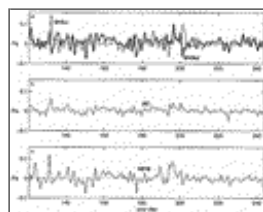
—, —, and —, 1997: Anticyclonic eddies trapped on the continental shelf by topographic irregularities. *J. Geophys. Res.*, **102**, 5625–5639..

Figures



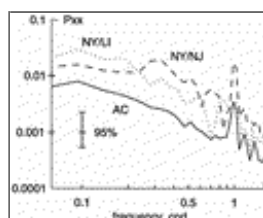
[Click on thumbnail for full-sized image.](#)

Fig. 1. Map of the southern part of the Mid-Atlantic Bight showing instrument sites used for this paper. From north to south MT: Montauk, NY: New York, SH: Sandy Hook, AC: Atlantic City, LW: Lewes, WP: Wachapreague, NF: Norfolk, and DK: Duck. Bars at the mooring locations show the principal axis orientation for currents (see text for details).



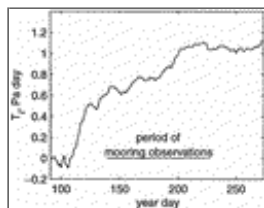
[Click on thumbnail for full-sized image.](#)

Fig. 2. Low-pass filtered time series of alongshore wind stress at (a) New York, heavy line: New Jersey coast and light line: Long Island coast; (b) Atlantic City; and (c) Norfolk (north of Cape Henry). Positive values denote upshelf stress component.



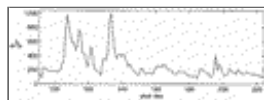
[Click on thumbnail for full-sized image.](#)

Fig. 3. Power spectra P_{xx} of alongshore wind stress [(Pa)²/day], solid line: Atlantic City; dashed line: New York/New Jersey; and dotted line: NY/Long Island.



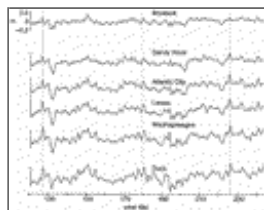
[Click on thumbnail for full-sized image.](#)

Fig. 4. Integral T_i of alongshore wind stress at Atlantic City.



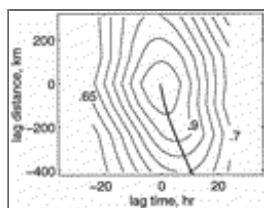
[Click on thumbnail for full-sized image.](#)

Fig. 5. Daily averaged Hudson River discharge measured at Waterford, New York.



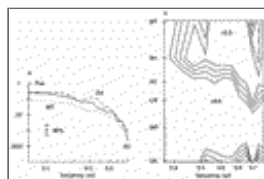
[Click on thumbnail for full-sized image.](#)

Fig. 6. Low-pass filtered adjusted sea level (ASL, in meters) time series from north (top of the plot) to south (bottom of the plot). Time series are arranged such that their axes are offset proportional to the alongshore distance between the stations.



[Click on thumbnail for full-sized image.](#)

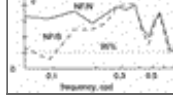
Fig. 7. Space- and time-lagged cross-correlation coefficients for adjusted sea level relative to Atlantic City. Contour interval is 0.05. Heavy line shows the locus of maximum correlation.



[Click on thumbnail for full-sized image.](#)

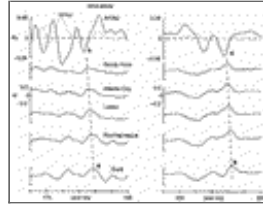
Fig. 8. Spectral analysis of adjusted sea level fluctuations: (a) power spectra P_{xx} of ASL ($m^2 \text{ day}^{-1}$) at Atlantic City (solid line), Montauk (dotted line) and Duck (dashed line); (b) coherence squared of ASL between Wachapreague and other tide gauge stations. Contours shown are 0.3, 0.4, 0.5, and 0.6, 95% confidence level for zero coherence is 0.21.





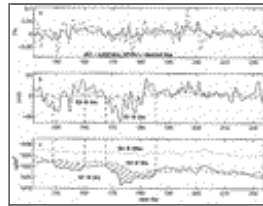
[Click on thumbnail for full-sized image.](#)

Fig. 9. Coherence squared between adjusted sea level at Duck and alongshore wind stress at (a) New York (solid line—NY/New Jersey, dashed line—NY/Long Island); (b) Atlantic City; (c) Norfolk (solid line—NF/north of Cape Henry; dashed line—NF/south of Cape Henry). Dotted lines show 95% confidence level for zero coherence.



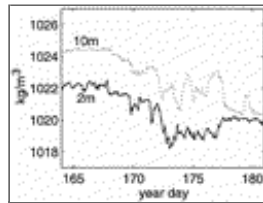
[Click on thumbnail for full-sized image.](#)

Fig. 10. Individual high-frequency sea level events in late June–early July (left panel) and in August (right panel). Time series of low-pass filtered alongshore wind stress (Pa) at New York (solid line: NY/New Jersey; dashed line: NY/Long Island) are shown at the top while time series of low-passed ASL (m) are below (stations arranged from north to south, top to bottom).



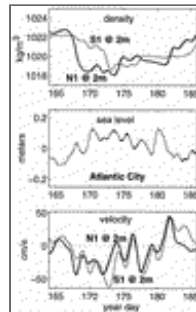
[Click on thumbnail for full-sized image.](#)

Fig. 11. Low-pass filtered time series of (a) alongshore wind stress, (b) alongshelf (principal axis) current components (upshelf direction is positive), and (c) water density. Vertical dashed lines and cross hatching show time intervals when enhanced buoyant flow was observed.



[Click on thumbnail for full-sized image.](#)

Fig. 12. Time series of water density (raw data) measured at mooring S1 at 2-m depth (solid line) and at 10-m depth (dotted line).



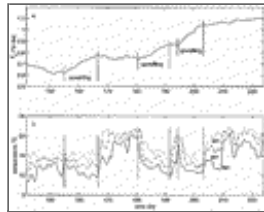
[Click on thumbnail for full-sized image.](#)

Fig. 13. Low-pass filtered time series of water density (top panel), sea level (middle panel), and alongshelf velocity (bottom panel) during the second period of enhanced buoyancy.



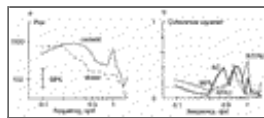
[Click on thumbnail for full-sized image.](#)

Fig. 14. Low-pass filtered time series measured at mooring N1: (a) alongshelf (principal axis) current component at 2-m depth; (b) normalized vertical difference of alongshelf currents between 2- and 4-m depth; (c) water density at depths 2, 4 and 8 m.



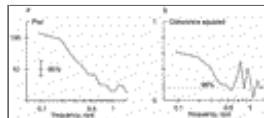
[Click on thumbnail for full-sized image.](#)

Fig. 15. (a) Integral T_i of alongshore wind stress at Atlantic City; (b) low-pass filtered time series of temperature measured at N1 mooring, solid line: at 8-m depth; dashed line: at 4-m depth; and dotted line: at 2-m depth. Vertical bars show time intervals of upwelling events.



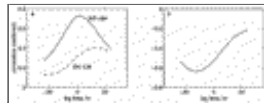
[Click on thumbnail for full-sized image.](#)

Fig. 16. (a) Power spectrum P_{xx} of alongshelf component of current [$(\text{m s}^{-1})^2/\text{day}$] measured at 4-m depth (solid line) and of the vertical shear of alongshelf current [$(10^{-2} \text{ s}^{-1})^2/\text{day}$] between 2 and 4 m (dashed line) at N1; (b) coherence squared between alongshelf current at N1, 4 m and alongshore wind component at Atlantic City (heavy line), New York/New Jersey (solid line), and New York/Long Island (dashed line).



[Click on thumbnail for full-sized image.](#)

Fig. 17. As for [Fig. 16](#) but for (a) temperature and (b) temperature and alongshelf wind component at Atlantic City.



[Click on thumbnail for full-sized image.](#)

Fig. 18. Time lagged cross-correlation coefficients between ASL at Wachapreague and (a) alongshelf difference in ASL fluctuations: WP–SH (solid line) and DK–LW (dashed line); (b) alongshelf wind stress at NF/N.

Corresponding author address: Dr. Alexander E. Yankovsky, Graduate College of Marine Studies, University of Delaware, Robinson Hall, Newark, DE 19716-3501.

E-mail: sasha@newark.cms.udel.edu

[top](#) ▲



amsinfo@ametsoc.org Phone: 617-227-2425 Fax: 617-742-8718
[Allen Press, Inc.](#) assists in the online publication of *AMS* journals.